USE OF VUV IMAGING TO EVALUATE COTR AND BEAM-STEERING EFFECTS IN A SASE FEL AT 130 NM*

A.H. Lumpkin**, Y.-C. Chae, R.J. Dejus, M. Erdmann, J.W. Lewellen, and Y. Li
Advanced Photon Source, Argonne National Laboratory, Argonne, Illinois 60439, USA

Abstract

We report the first experimental data on coherent optical transition radiation (COTR) at 130 nm as well as first tests of the analytical model for single-kick-error effects on gain in a SASE FEL. We use both near-field and far-field imaging of the SASE radiation. We also use the COTR near-field data to identify a calibration factor error in the rf BPM system so that the SKE analysis is based on the camera centroid positions and their relation to those of the alignment laser only.

INTRODUCTION

We have continued to explore VUV operations on the Advanced Photon Source (APS) self-amplified emission (SASE) free-electron laser (FEL) [1]. With installation of a fifth VUV imaging station located after undulator 7 of an eight-undulator series, we have performed our most complete SASE gain curve measurements at 130 nm as well as obtaining beam profile, position, and divergence information. This is the shortest wavelength to date for our complementary coherent optical transition radiation (COTR) measurements [2]. We have also done the first experimental test of Tanaka et al.'s analytical model for the effects of a single-kick error of the e-beam on gain and microbunching in a SASE FEL [3]. In the course of the experiments, we performed a direct comparison of the beam position as determined by the local rf BPMs and the VUV video cameras. An rf BPM calibration factor error was determined so all steering data were evaluated using the COTR near-field image centroids obtained from the cameras adjacent to and one undulator downstream of the selected horizontal corrector in the single-kick error tests. In addition, we compared the e-beam image centroid positions with those of the alignment laser at the available cameras to sort out the effective trajectory and its effect on overall gain. The FEL performance was consistent with GENESIS simulations of the experiment described in detail in a companion paper [4].

EXPERIMENTAL BACKGROUND

The APS injector system for the storage ring includes an S-band linac that can be configured with the photocathode (PC) rf gun to provide bright beams to the FEL. The drive laser is a Nd:YLF oscillator with an amplifier, and the fundamental frequency is quadrupled to attain laser light at 266 nm. The PC gun was operated with a Cu photocathode at the time of these experiments [5]. Typically, about 300 pC of charge were accelerated and then bunch compressed in a chicane where the beam energy is 150 MeV [6]. The normalized emittance $\varepsilon_{x,y}$ = 4.5/3.5 mm mrad was measured after the chicane, and the bunch length was measured with a zero-phasing rf technique to be about 200 fs (rms). The beam is further transported to the low-energy undulator test line (LEUTL) tunnel where eight, 2.4-m-long undulators are installed. The gun, linac, and undulator system are schematically shown in Fig. 1, and the e-beam parameters are summarized in Table 1.

Before and after each undulator station we have a quadrupole, steering correctors, rf BPMs, and visible light imaging station. The quadrupole and horizontal and vertical correctors are located first in the drift space followed by the rf BPM buttons. For the purpose of these experiments we used the five VUV imaging stations installed after undulator numbers 2, 4, 5, 6, and 7 and denoted as VUV-2, etc. As shown in Fig. 2, the station included a first actuator that has a YAG:Ce screen, a thin Al foil option, and pinhole reference target. At a

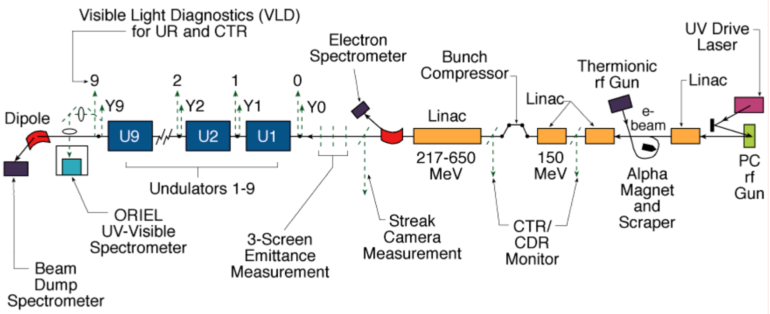

Figure 1: A schematic of the APS SASE FEL showing the PC gun, linac, bunch compression stage, three-screen emittance matching station, and the undulator series with diagnostics.

* Work supported by the U.S. Department of Energy, Office of Basic Energy Sciences, under Contract No. W-31-109-ENG-38.
**lumpkin@aps.anl.gov

Table 1: Nominal Electron Beam Parameters with the PC-gun Beam Injected into the Undulators during the Experiments

Parameter	Value
Beam Energy (MeV)	439
Emittance x,y (mm-mrad)	4-6
Peak Current (A)	300 to 500
Bunch Length (ps rms)	0.3
Charge (pC)	300-400
Energy Spread (%)	0.1-0.2

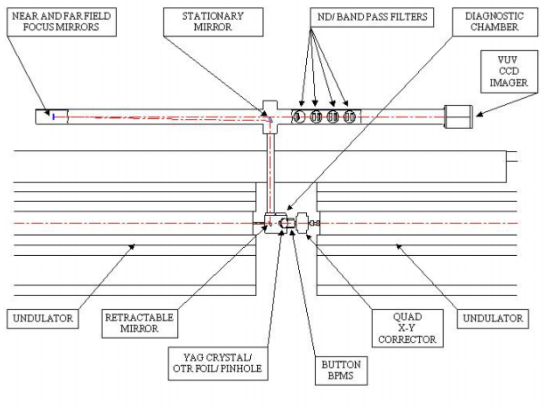

Figure 2: A schematic of the upgraded diagnostic stations for VUV imaging after undulators 2, 4, 5, 6, and 7. The quadrupole with H and V correctors, the rf BPM, the first actuator stage, the 45° retractable mirror, and reflective optics to the VUV camera are shown.

distance of 63 mm downstream a second pick-off mirror is located on a stepper motor. In one position the mirror surface is oriented to send optical radiation to the UV-visible cameras on the wall and the other position directs radiation upward into the VUV transport. A fixed mirror redirects the radiation to one of two selectable spherical mirrors of focal length 900 and 2000 mm that provide near-field and far-field imaging, respectively, for the VUV CCD camera. A series of stepper motors located between the spherical mirror and camera control the selectable filter assemblies, which include visible light bandpass filters, neutral density (ND) filters, VUV bandpass filters, and VUV regime attenuation. The CCD camera is a Roper Scientific model with a 512 × 512 pixel array sensor, which detects radiation from about 120 nm through the visible regime [7] with a well depth of 10^5. The camera is based on the Marconi VUV EEV57-10 back-thinned chip with no antireflection coating and can transfer the full image at a maximum rate of 3 Hz. The data are digitized by a 16-bit board and saved on a local PC disk. Usually, we acquire 100 images for each z-position or angular kick position. The images are subsequently transferred to the UNIX system and processed off-line with GIANT or J Data Miner [8], local programs with an IDL base. Background subtractions are performed and the integrated intensities in a prescribed region-of-interest are determined. We also obtain the projected profile centroids and sizes at FWHM.

The single-kick-error experiments were performed in the undulator 5 region by turning off the quadrupole (Q5) and corrector (H5) after the undulator and using the H4 corrector before the undulator. The first test was to establish the amount of steering strength by assessing the rf BPM readings and the VUV-4 and VUV-5 camera readings.

RESULTS AND DISCUSSION

The experiments were initiated with a z-dependent gain scan following the tune-up through each of the five VUV stations. The near-field gain curve is presented in Fig. 3 which was not available during the experiment. From the selected VUV attenuators as a function of z, we assessed that we were in the exponential gain regime at undulator 5 so we could test the model.

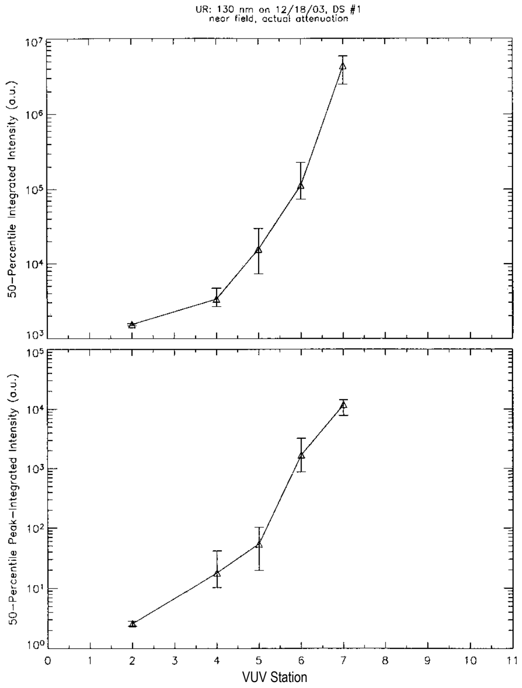

Figure 3: Results of the z-dependent gain measurement.

As part of the steering tests, the recorded rf BPM positions before and after undulator 5 were tracked with steering strength of H4. The results are shown in Fig. 4. However, when we compared the deflections to the VUV image centroids with H4 settings, we ascertained that the rf BPM calibration factor was too low by a factor of six. Since the VUV camera's images were clearly moving beam diameter distances and the calibration factor of the camera had been confirmed by using the stepper motor to move the pinhole target position a known amount, we decided to rely on the VUV camera images. Examples of the image position changes are given in Table 2, where the calibration factor is 11 μm/channel, and in Fig. 5. The effective kick angle is shown in Fig. 5 (bottom) with an average of ~0.3 mrad per Amp of corrector strength. We also had recorded the alignment laser image positions in each camera so we could reference the e-beam position to the “straightline” of the alignment laser. The final results indicate that in the undulator 5 region the beam trajectory is actually fairly close to the alignment laser (within 50 μrad) so the analytical model should apply.

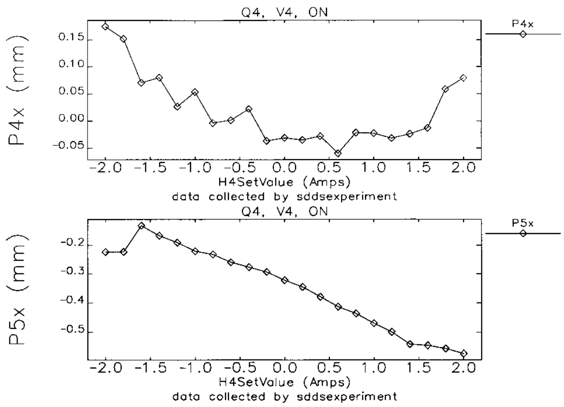

Figure 4: Results of the rf BPM readings versus H4 corrector strength. The reported deflections are found to be too small compared to VUV image centroids.

Table 2: Summary of Image Centroid Positions at VUV-5 versus Corrector Setting (12-18-03)

Note: Foil in, ND0.0, Q_5 off: H5 off

File #	Q4:V4	H4 (A)	X_c*	D_x*	Y_c*	D_y*
4228	On	-2	37	---	120	
4244	On	0	161	124	126	6
4249	On	2	290	129	117	-9
4259	Off	2	252		224	
4268	Off	0	115	-137	218	-6
4278	Off	-2	(4)		229	11

*Positions in channels (ch) at 11 μm per ch.

Note: When turn off Q4/V4 with H_4=0, the image moves -46 ch = -500 μm in x. V4 was at -1.7A in tuned state, and we have a vertical motion down of 109 ch = 1100 μm.

The SKE model of Tanaka et al., [3] defines the new SASE gain length L'_g in terms of a critical angle, $\theta_c = \sqrt{\lambda/Lg}$, where λ is the wavelength of the SASE and L_g is gain length at zero error. We can rewrite this as

$$L'_g = \frac{L_g}{1-x^2} \quad \text{where } x = \theta/\theta_c\,, \qquad (1)$$

and θ is the kick angle. The camera steering data are given in Figs. 5 and 6. In Fig. 6 the ratio of P5/P4 represents the ratio of the VUV-5/VUV-4 image intensities. By steering the beam close to one half the critical angle, the gain is reduced by a factor of two under these conditions. Any offset, x_0, is to be determined. In addition, this model addressed a smearing of the microbunching, which would cause a change in its gain length L_g to

$$L''_g = \frac{L_g}{1-\pi x^2}\,, \quad \text{where } L_g \text{ is the SASE gain length.} \qquad (2)$$

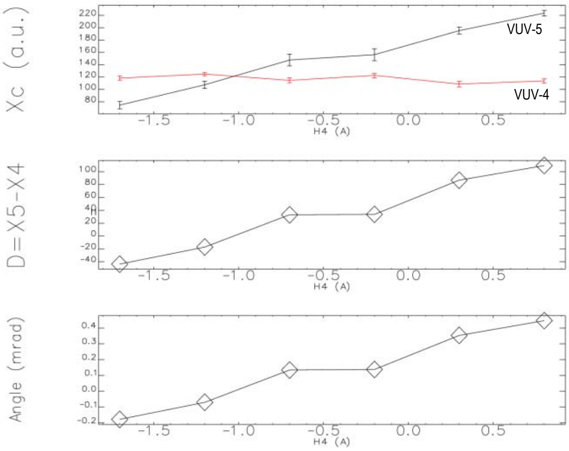

Figure 5: Results of the VUV-4 and VUV-5 camera image centroid shifts (top), the position difference in the two cameras (middle), and the effective kick angle (bottom) versus H4 corrector strength.

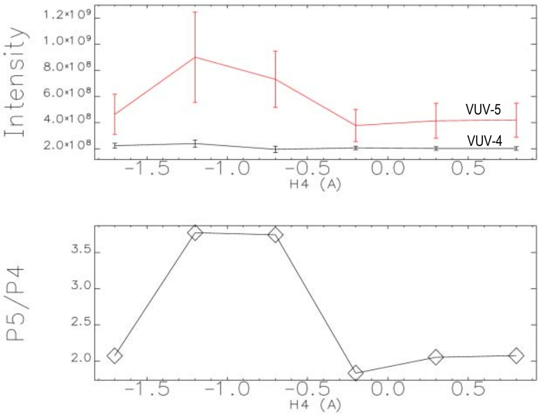

Figure 6: The measured image intensities for VUV-4 and VUV-5 versus H4 corrector strength (top) and the basic ratio P5/P4 of VUV-5/VUV-4 for the SASE undulator light with far-field imaging (bottom).

The multiplier of π in the denominator on x^2 causes a more rapid reduction in gain length versus θ, but the curve is also only a bound on the inner θ limit. However, at the low gains at the time of the experiment the far-field images were too weak and the near-field images may have a contribution from the broadband UV-visible OTR light. We have repeated the experiments with rf thermionic gun beam recently and will continue this evaluation of microbunch smearing as detected by COTR signals.

SUMMARY

In summary, we have extended our COTR experiments to 130 nm. The near-field images were used in the single-kick error tests to determine beam steering instead of the rf BPMs whose calibration was found to be incorrect. The comparisons of VUV SASE gain to steering error were found to be in agreement with the model and GENESIS simulations as described in more detail in a companion paper [4]. The test of the microbunching smearing effect in the model was experimentally less clear, and further experiments and analysis are warranted.

ACKNOWLEDGEMENTS

The authors acknowledge the support of Kwang-Je Kim and the Advanced Accelerator Research Initiative at Argonne National Laboratory.

REFERENCES

[1] S.V. Milton et al., Science 292 (2002) 2037.
[2] A.H. Lumpkin et al., "First Observations of COTR due to a Microbunched Beam in the VUV at 157 nm," Nucl. Instrum. Methods (in press 2004).
[3] T. Tanaka et al., "Consideration on an Alignment Tolerance of BPMs for SCSS Undulator Line," Nucl. Instrum. Methods (in press 2004).
[4] Y.-C. Chae et al., "An Experimental Study of the Beam-Steering Effect on FEL Gain at LEUTL's Segmented Undulator," (these proceedings).
[5] S. Biedron et al., Proc. of 1999 Particle Accelerator Conference, New York, NY, 2024-2026 (1999).
[6] M. Borland et al., A.W. Chao (Ed.), Proc. of the 2000 Linac Accelerator Conference, Monterey, CA, SLAC R561, 863 (2001).
[7] P. Den Hartog et al., Nucl. Instrum. Methods, A483, 407 (2002).
[8] B. Tiemann, J Data Miner analysis program, ANL, (2003).